



Article

Gold-Nanoparticle-Deposited TiO₂ Nanorod/Poly(Vinylidene Fluoride) Composites with Enhanced Dielectric Performance

Pornsawan Kum-onsa ¹, Narong Chanlek ², Jedsada Manyam ³ , Prasit Thongbai ^{4,5,*} , Viyada Harnchana ^{4,5} , Nutthakritta Phromviyo ⁶ and Prinya Chindaprasirt ⁶

¹ Materials Science and Nanotechnology Program, Faculty of Science, Khon Kaen University, Khon Kaen 40002, Thailand; pornsawan.kumonsa@gmail.com

² Synchrotron Light Research Institute (Public Organization), 111 University Avenue, Muang District, Nakhon Ratchasima 30000, Thailand; Narong@slri.or.th

³ Nanotechnology Center (NANOTEC), National Science and Technology Development Agency (NSTDA), Pathum Thani 12120, Thailand; jedsada@nanotec.or.th

⁴ Department of Physics, Faculty of Science, Khon Kaen University, Khon Kaen 40002, Thailand; viyada@kku.ac.th

⁵ Institute of Nanomaterials Research and Innovation for Energy (IN-RIE), NANOTEC-KKU RNN on Nanomaterials Research and Innovation for Energy, Khon Kaen University, Khon Kaen 40002, Thailand

⁶ Sustainable Infrastructure Research and Development Center, Department of Civil Engineering, Faculty of Engineering, Khon Kaen University, Khon Kaen 40002, Thailand; nutthaphrom@gmail.com (N.P.); prinya@kku.ac.th (P.C.)

* Correspondence: pthongbai@kku.ac.th



Citation: Kum-onsa, P.; Chanlek, N.; Manyam, J.; Thongbai, P.; Harnchana, V.; Phromviyo, N.; Chindaprasirt, P. Gold-Nanoparticle-Deposited TiO₂ Nanorod/Poly(Vinylidene Fluoride) Composites with Enhanced Dielectric Performance. *Polymers* **2021**, *13*, 2064. <https://doi.org/10.3390/polym13132064>

Academic Editor: Jung-Chang Wang

Received: 18 June 2021

Accepted: 21 June 2021

Published: 23 June 2021

Publisher's Note: MDPI stays neutral with regard to jurisdictional claims in published maps and institutional affiliations.



Copyright: © 2021 by the authors. Licensee MDPI, Basel, Switzerland. This article is an open access article distributed under the terms and conditions of the Creative Commons Attribution (CC BY) license (<https://creativecommons.org/licenses/by/4.0/>).

Abstract: Flexible dielectric polymer composites have been of great interest as embedded capacitor materials in the electronic industry. However, a polymer composite has a low relative dielectric permittivity ($\epsilon' < 100$), while its dielectric loss tangent is generally large ($\tan\delta > 0.1$). In this study, we fabricate a novel, high-permittivity polymer nanocomposite system with a low $\tan\delta$. The nanocomposite system comprises poly(vinylidene fluoride) (PVDF) co-filled with Au nanoparticles and semiconducting TiO₂ nanorods (TNRs) that contain Ti³⁺ ions. To homogeneously disperse the conductive Au phase, the TNR surface was decorated with Au-NPs ~10–20 nm in size (Au-TNRs) using a modified Turkevich method. The polar β -PVDF phase was enhanced by the incorporation of the Au nanoparticles, partially contributing to the enhanced ϵ' value. The introduction of the Au-TNRs in the PVDF matrix provided three-phase Au-TNR/PVDF nanocomposites with excellent dielectric properties (i.e., high $\epsilon' \approx 157$ and low $\tan\delta \approx 0.05$ at 1.8 vol% of Au and 47.4 vol% of TNRs). The ϵ' of the three-phase Au-TNR/PVDF composite is ~2.4-times higher than that of the two-phase TNR/PVDF composite, clearly highlighting the primary contribution of the Au nanoparticles at similar filler loadings. The volume fraction dependence of ϵ' is in close agreement with the effective medium percolation theory model. The significant enhancement in ϵ' was primarily caused by interfacial polarization at the PVDF–conducting Au nanoparticle and PVDF–semiconducting TNR interfaces, as well as by the induced β -PVDF phase. A low $\tan\delta$ was achieved due to the inhibited conducting pathway formed by direct Au nanoparticle contact.

Keywords: gold nanoparticle; titanium dioxide nanorod; poly(vinylidene fluoride); heat treatment; hybrid nanoparticle; modified Turkevich method

1. Introduction

With recent developments in the electronic industry, dielectric polymer composite materials have attracted increasing interest for a wide range of applications, such as energy storage devices, dielectric capacitors, and electromechanical actuators [1,2]. Poly(vinylidene fluoride) (PVDF) has been used as a dielectric polymer material due to its high energy density, high electric break down field, and flexibility [3,4]. However, the relative dielectric permittivity (ϵ') of PVDF is too low (≈ 10 [3]) for electronic applications.

Many studies have attempted to fabricate polymer composites with high ϵ' values by incorporating fillers into the PVDF matrix. Two-phase ceramic/polymer and metal/polymer composites have been synthesized and widely studied for improving the dielectric performance of polymer composite materials [5–11]. Several ceramic/polymer composites, such as $\text{CaCu}_3\text{Ti}_4\text{O}_{12}$ /PVDF [5,12], $\text{CaCu}_3\text{Ti}_4\text{O}_{12}$ /polystyrene [13], BaTiO_3 /PVDF [6], $\text{Ba}_{0.5}\text{Sr}_{0.5}\text{TiO}_3$ /P(VDF-CTFE) [14], and $\text{Ba}_{0.6}\text{Sr}_{0.4}\text{TiO}_3$ /PVDF [15], have high ϵ' values (~50–80 at 1 kHz). The ϵ' of a ceramic/polymer composite is generally below 100 even at a high ceramic loading (50 vol%), while its dielectric loss tangent ($\tan\delta$) is also elevated (>0.1 at 1 kHz and ~25 °C) [5,16]. However, metal/polymer composites, such as Ni/PVDF, Ni/P(VDF-CTFE) [17,18], MWCNT/PVDF [8,19], and Ag/PVDF [7,20], can exhibit significantly higher ϵ' at low concentrations of conducting fillers than ceramic/PVDF composites. It is difficult to maintain the filler loading at the percolation threshold (f_c) to achieve a high relative permittivity. Metal/polymer composites generally exhibit significantly large $\tan\delta$ and electrical conductivity (σ) values at f_c . It should be noted that the metal/polymer composites with extreme ϵ' values also have high $\tan\delta$ and σ , which limits the practical applications of these metal/polymer composites.

Owing to such challenges, developing polymer composites with high ϵ' and low $\tan\delta$ values is desirable. Several researchers have studied and reported three-component composites comprising metal, ceramic, and polymer matrices, such as $\text{Ba}(\text{Fe}_{0.5}\text{Nb}_{0.5})\text{O}_3$ /Ni/PVDF, Ni/ $\text{CaCu}_3\text{Ti}_4\text{O}_{12}$ /PVDF, Ni/ BaTiO_3 /PVDF, $\text{Na}_{0.5}\text{Bi}_{0.5}\text{Cu}_3\text{Ti}_4\text{O}_{12}$ /MWCNTs/PVDF, and Ag/ $\text{Na}_{0.5}\text{Bi}_{0.5}\text{Cu}_3\text{Ti}_4\text{O}_{12}$ [21–25]. In particular, a novel composite with structured hybrid fillers has been of great interest. Recently, many studies on PVDF-based composites filled with hybrid nanoparticles have been reported. Luo et al. [26] reported a novel polymer composite filled with Ag- BaTiO_3 hybrid nanoparticles. This Ag- BaTiO_3 /PVDF composite exhibited a high ϵ' (160) with $\tan\delta \approx 0.11$ at a filler volume fraction ($f_{\text{Ag-BT}}$) of 0.568. This $\tan\delta$ value is much lower than those reported in many conventional three-phase polymer composites; unfortunately, it is still much larger than 0.05, which is an acceptable value for capacitor applications. Although incorporating Ag- BaTiO_3 hybrid nanoparticles can increase the ϵ' of a composite, the ϵ' of ferroelectric BaTiO_3 is generally strongly dependent on its Curie temperature. Furthermore, most ferroelectric oxides are piezoelectric, which results in mechanical resonance in the device during charging and discharging, thereby limiting its reliability [27].

Rutile- TiO_2 is one of the most widely used oxides in electronic materials, sensors, and semiconductors [28,29]. Furthermore, rutile- TiO_2 can exhibit colossal dielectric properties when a minor portion of Ti^{4+} is reduced to Ti^{3+} due to the existence of oxygen vacancies and/or substitution by pentavalent ions (e.g., Nb^{5+} or Ta^{5+}). Polaron-like electron hopping between Ti^{3+} and Ti^{4+} ions can cause a significant increase (by a factor of $\sim 10^4$) in dielectric permittivity [30]. Since TiO_2 is not a ferroelectric ceramic, TiO_2 nanoparticles were used as a filler in various polymer composites [31–33]. Unfortunately, the ϵ' values of the TiO_2 /polymer composites are still significantly low owing to the low ϵ' of the TiO_2 nanoparticles. Polymer composites filled with modified TiO_2 nanoparticles such as Ag- TiO_2 hybrid particles and Ag@ TiO_2 core-shell structures were developed to enhance ϵ' [34–37]. Although these composites can exhibit high ϵ' values of ~60–150, large $\tan\delta$ values are generally obtained (~0.1–1) at high filler concentrations (70 vol%) [34,35]. Among various metal nanoparticles, gold nanoparticles are widely used as fillers to improve the insulation properties of polymer materials because they are nontoxic and less likely to be oxidized [38]. A significantly enhanced ϵ' (~54–118) and low $\tan\delta$ (<0.06) were achieved in Au- BaTiO_3 /PVDF [39] and Au- BiFeO_3 /PVDF, with only a small amount of Au in the third phase of each polymer composite ($f_{\text{Au}} < 0.02$) [40]. According to previous works [39,40], the Au- BaTiO_3 /PVDF and Au- BiFeO_3 /PVDF composites not only exhibited high ϵ' values, but their $\tan\delta$ and σ were also suppressed due to the incorporation of the Au nanoparticles. Therefore, the conductive Au phase nanoparticle is one of the most interesting conductive phases for use as a filler in three-phase polymer composites.

To the best of our knowledge, there is a lack of substantial information on polymer composites incorporated with Au-TiO₂ hybrid nanoparticles. Therefore, in this study we aimed to fabricate a novel nanocomposite comprising a PVDF polymer matrix, Au nanoparticles, and TiO₂ nanorods (TNRs). TNRs have higher surface areas than spherical TiO₂; therefore, they lead to stronger interfacial polarization and a significantly enhanced ϵ' . Herein, Au-TNR/PVDF nanocomposites with enhanced ϵ' and low $\tan\delta$ were fabricated. A modified Turkevich method was used to attach Au onto the surfaces of the TNRs. The Au-TNR/PVDF nanocomposites were prepared through liquid-phase-assisted dispersion and hot-pressing methods. Several properties of these nanocomposites such as their morphologies, microstructures, phase structures, chemical stages, and dielectric properties were investigated, and the significantly improved dielectric properties of the nanocomposites are discussed.

2. Experimental Section

2.1. Preparation of Heat-Treated TNRs

TNRs (99.5% purity) with particle size <100 nm were purchased from Sigma-Aldrich. Heat treatment at 500 °C for 3 h in air was performed on the TNRs to evaporate the moisture.

2.2. Preparation of Au-TNR Hybrid Nanoparticles

Au-TNR hybrid nanoparticles were prepared through a modified Turkevich method. The corresponding procedure is described as follows: heat treatment of TNR powder was carried out by ultrasonically dispersing the powder in deionized water for 30 min. Then, the white TNR suspension was stirred using a magnetic stirrer at ~25 °C for 30 min, after which 1 mM HAuCl₄·3H₂O was dissolved in the TNR solution under constant stirring. After the solution was heated to 300 °C, 38.8 mM of sodium citrate (>99.0%, Sigma-Aldrich) solution was dissolved in the TNR solution. To ensure a complete reaction, the suspension was stirred until its color changed from white to purple. The purple suspension was sequentially cooled to room temperature, centrifuged at 8500 rpm, and washed several times with deionized water. Finally, Au-TNR hybrid nanoparticles were obtained without agglomeration by freeze-drying.

2.3. Preparation of Au-TNR/PVDF Nanocomposites

Au-TNR/PVDF nanocomposites containing Au-TNR fillers with different f_{Au} and f_{TNRs} values were prepared through liquid-phase-assisted dispersion and hot-pressing methods. First, Au-TNR hybrid nanoparticles and the PVDF powder ($M_w \sim 534,000$, Sigma-Aldrich) were mixed by ball-milling with ZrO₂ in ethanol for 3 h. Second, the mixture was dried at 80 °C to evaporate ethanol, after which the mixed powder was pressed at 200 °C for 30 min at 10 MPa. Finally, the Au-TNR/PVDF nanocomposite sample, with a diameter and thickness of ~12 mm and ~0.5–1 mm, respectively, was obtained at room temperature. Au-TNR/PVDF nanocomposite samples with $f_{Au-TNRs} = 0.094, 0.216, 0.294, 0.383, 0.492,$ and 0.624 are referred to as Au-TNRs/PVDF-1, Au-TNRs/PVDF-2, Au-TNRs/PVDF-3, Au-TNRs/PVDF-4, Au-TNRs/PVDF-5, and Au-TNRs/PVDF-6, respectively. The separated volume fractions of Au and TNRs for each composite sample are listed in Table 1.

Table 1. Volume fraction of Au (f_{Au}), TNRs (f_{TNRs}), Au-TNRs ($f_{Au-TNRs}$), ϵ' , $\tan\delta$, and σ_{ac} at 1 kHz and room temperature for nanocomposites with varying filler amounts.

Sample	f_{Au}	f_{TNRs}	$f_{Au-TNRs}$	ϵ'	$\tan\delta$	σ_{ac} (10^{-11} S·cm $^{-1}$)
PVDF	0	0	0	10.8	0.020	4.1
Au-TNR/PVDF-1	0.005	0.089	0.094	29.1	0.012	20.3
Au-TNR/PVDF-2	0.010	0.206	0.216	37.1	0.028	59.1
Au-TNR/PVDF-3	0.013	0.281	0.294	53.8	0.062	188.6
Au-TNR/PVDF-4	0.016	0.367	0.383	57.7	0.075	242.8
Au-TNR/PVDF-5	0.018	0.474	0.492	156.7	0.048	427.7
Au-TNR/PVDF-6	0.021	0.603	0.624	226.3	0.052	657.6
TNR/PVDF	0	0.5	0	65.9	0.028	103.5

2.4. Characterization

The phase structures of the PVDF filler and Au-TNR/PVDF nanocomposites were characterized by X-ray diffractometry (XRD, PANalytical, EMPYREAN). The surface morphologies of Au, TNRs, and the Au-TNR nanoparticles were revealed using transmission electron microscopy (TEM, FEI Tecnai G2 20). The chemical composition of each element in the Au-TNR hybrid nanoparticles was analyzed by X-ray photoelectron spectroscopy (XPS, PHI5000 VersaProbe II, ULVAC-PHI, Japan) at the SUT-NANOTEC-SLRI Joint Research Facility, Synchrotron Light Research Institute (SLRI), Thailand. The fracture microstructures, distributions, and percentages of each element in the Au-TNR/PVDF nanocomposites were investigated by focused ion beam–field emission scanning electron microscopy (FIB–FESEM, FEI Helios Nanolab G3 CX). The samples were fractured using liquid N₂ and their surfaces were sputtered with Au before SEM characterization. The crystalline phases of the nanocomposites were determined using Fourier-transform infrared spectroscopy (FTIR, Bruker, TENSOR27) in the 700–1800 cm⁻¹ wavelength range. The dielectric properties of the samples were analyzed using an impedance analyzer (KEYSIGHT E4990A) in the 10²–10⁶ Hz and –60–150 °C frequency and temperature ranges, respectively, with an oscillation voltage of 0.5 V. Before any dielectric measurement, both sides of each circular sample were coated with Ag to form electrodes.

3. Results and Discussion

Figure 1 displays TEM images showing the morphologies of the Au, TNRs, and Au-TNR hybrid nanoparticles. The Au nanoparticles are spherical with diameters of 10–20 nm. Meanwhile, the heat-treated TNRs are rod-shaped with slightly different aspect ratios, while some Au clusters are dotted on the TNR surfaces of the Au-TNR hybrid nanoparticles, revealing that the Au nanoparticles successfully formed on the TNR surfaces.

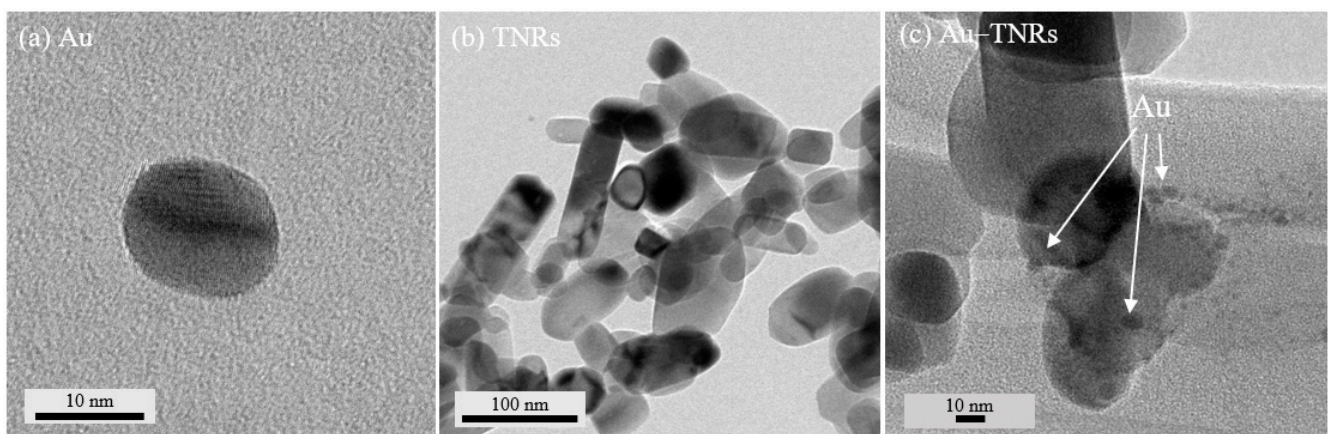
**Figure 1.** TEM images of (a) Au, (b) TNRs, and (c) Au-TNR hybrid nanoparticles.

Figure 2 shows XPS spectra of the Au-TNR powder. As shown in Figure 2a, Au 4f peaks were observed at 83.33 and 86.98 eV, which are assigned to Au 4f_{7/2} and Au 4f_{5/2}, respectively [41,42]. This confirmed the existence of Au in the prepared Au-TNR powder. As shown in Figure 2b, small Ti 2p peaks were observed at binding energies of 457.69 and 461.34 eV, respectively, corresponding to the presence of Ti³⁺. Ti 2p signals was observed at binding energies of 458.75 and 464.41 eV, indicating the presence of Ti⁴⁺ [43]. The Ti³⁺/Ti⁴⁺ ratio was found to be 7.52%. Figure 2c shows three of O 1s XPS peaks; the peak at 529.99 eV can be attributed to the oxygen lattice (Ti–O) [28,43]. Additional peaks were observed at 531.29 and 532.32 eV, which can be attributed to the oxygen vacancy in the rutile structure [28] and hydroxyl groups [43], respectively. The detected Ti³⁺ in the Au-TNR powder is likely to have originated from oxygen vacancies, which can be explained by Equations (1) and (2).



The presence of the Ti³⁺ ions can cause a significant increase in conductivity, thereby leading to electron hopping between the Ti³⁺ and Ti⁴⁺ ions under an applied electric field. The XPS results confirmed the existence of Au, Ti³⁺, and oxygen vacancies, which affected ϵ' enhancement in the Au-TNR/PVDF nanocomposites.

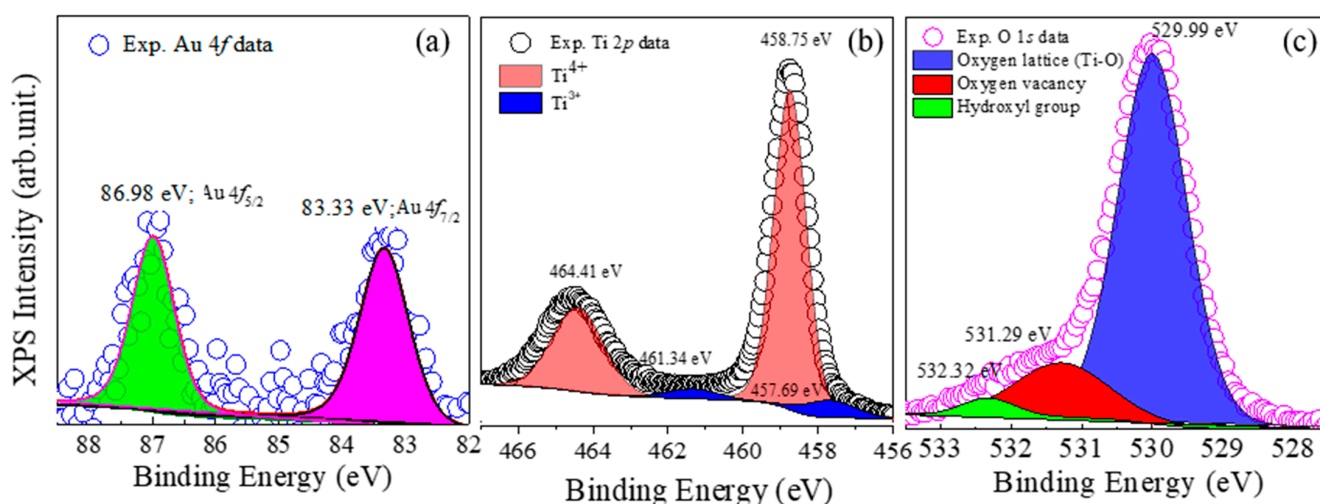


Figure 2. XPS spectra of Au-TNR hybrid nanoparticles; (a) Au 4f, (b) Ti 2p, and (c) O 1s.

The XRD patterns of Au, PVDF, TNRs, Au-TNR nanoparticles, and Au-TNR/PVDF nanocomposites were obtained in the 10–80° 2 θ range, as shown in Figure 3. The XRD pattern of the PVDF polymer corresponds to the (100), (020), (110), and (021) planes of the α -phase [4]. The XRD pattern of the TNRs showed peaks similar to those of the tetragonal structure of the rutile phase according to the standard reported in JCPDS 21-1276; no impurity phase was detected. In the case of the Au-TNR hybrid nanoparticles and Au-TNR/PVDF nanocomposites, the XRD peak for Au can be observed at 2 θ \approx 38.11 and assigned as a (111) plane (JCPDS 00-00-1172), confirming the existence of Au in the hybrid particles and Au-TNR/PVDF nanocomposites. Therefore, the Au nanoparticles were confirmed to exist in the Au-TNR nanoparticles and Au-TNR/PVDF nanocomposites. Meanwhile, no PVDF diffraction peaks were observed in the Au-TNR/PVDF nanocomposite sample, which can be attributed to the semicrystalline nature of PVDF, which is shielded by the stronger crystalline diffraction intensity of the TNRs compared to PVDF.

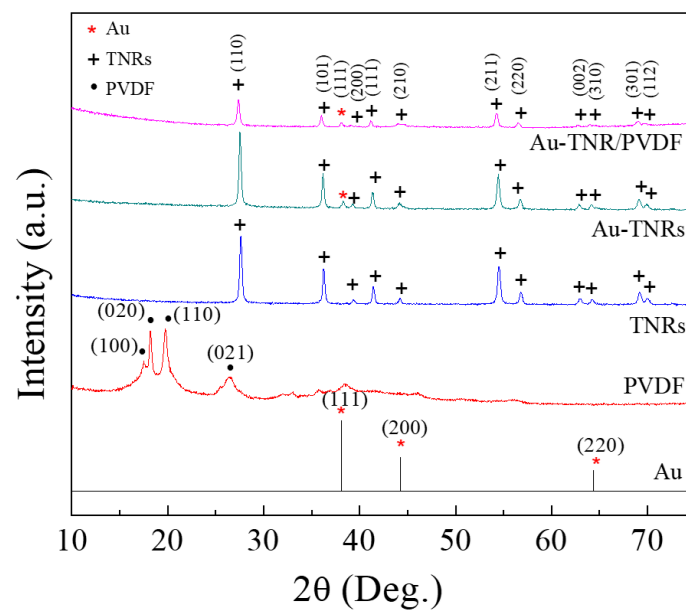


Figure 3. XRD patterns of the Au standard data Au standard (JCPDS 00-00-1172), TNRs, fabricated Au-TNR hybrid nanoparticles, and Au-TNR/PVDF-4 nanocomposite.

The FTIR spectra of the PVDF polymer nanocomposites filled with the TNRs and Au-TNRs are shown in Figure 4. Both nanocomposite systems consisted of α -, β -, and γ -PVDF phases. Weak transmittance bands observed at 766 and 976 cm^{-1} are attributed to the nonpolar α -phase [4], consistent with the XRD result (Figure 3). As the characteristic bands of the β - and γ -phase overlapped at 840 cm^{-1} , they were difficult to distinguish. However, the characteristic band at 1279 cm^{-1} only corresponds to the β -phase [4]. As shown in Figure 4, the transmittance intensity of the β -phase for the three-phase Au-TNR/PVDF-5 composite is stronger than that of the two-phase TNR/PVDF composite, particularly at 1279 cm^{-1} . To estimate the % β -phases in the nanocomposites, the absorption ratios of the β - and α -phase were compared. Equation (3) was used to quantify the relative fraction of the β -phase ($F(\beta)$) [4], assuming that only the β - and α -phase exist:

$$F(\beta) = \frac{A_{\beta}}{(K_{\beta}/K_{\alpha})A_{\alpha} + A_{\beta}} \quad (3)$$

where A_{α} and A_{β} are the absorption bands at 766 and 840 cm^{-1} , respectively, and K_{α} and K_{β} are the absorption coefficients of the respective bands ($K_{\alpha} = 6.1 \times 10^4$ and $K_{\beta} = 7.7 \times 10^4$ $\text{cm}^2 \cdot \text{mol}^{-1}$). The calculated $F(\beta)$ of the two-phase and three-phase nanocomposites were 0.220 and 0.331, respectively. The negative charge of the Au nanoparticles causes an increase in amount of the polar β -phase of the PVDF nanocomposites [44], leading to a Au-TNR/PVDF nanocomposite with a significantly enhanced ϵ' [45].

The fracture cross-sectional images of the nanocomposites containing various Au-TNR hybrid particles are shown in Figure 5. The microstructure of the PVDF polymer is shown in Figure 5a and reveals that the PVDF molecules form a continuous phase. Figure 5b,c show the microstructures of the Au-TNRs/PVDF-2 and Au-TNRs/PVDF-4 nanocomposites. The Au-TNR hybrid nanoparticles are dispersed homogeneously in the PVDF matrix without aggregation. Some air voids and Au-TNR nanoparticle aggregation were observed with increasing Au-TNR hybrid particle content, as exemplified by Au-TNR/PVDF-6, as shown in Figure 5d.

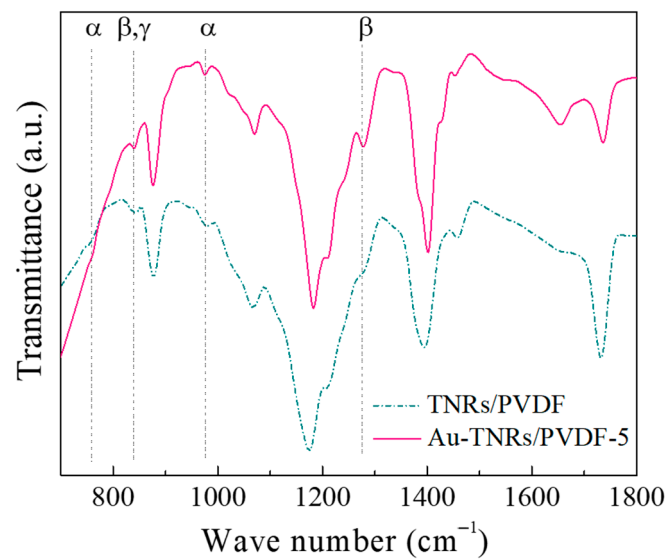


Figure 4. FTIR spectra of the TNR/PVDF and Au-TNR/PVDF-5 nanocomposites.

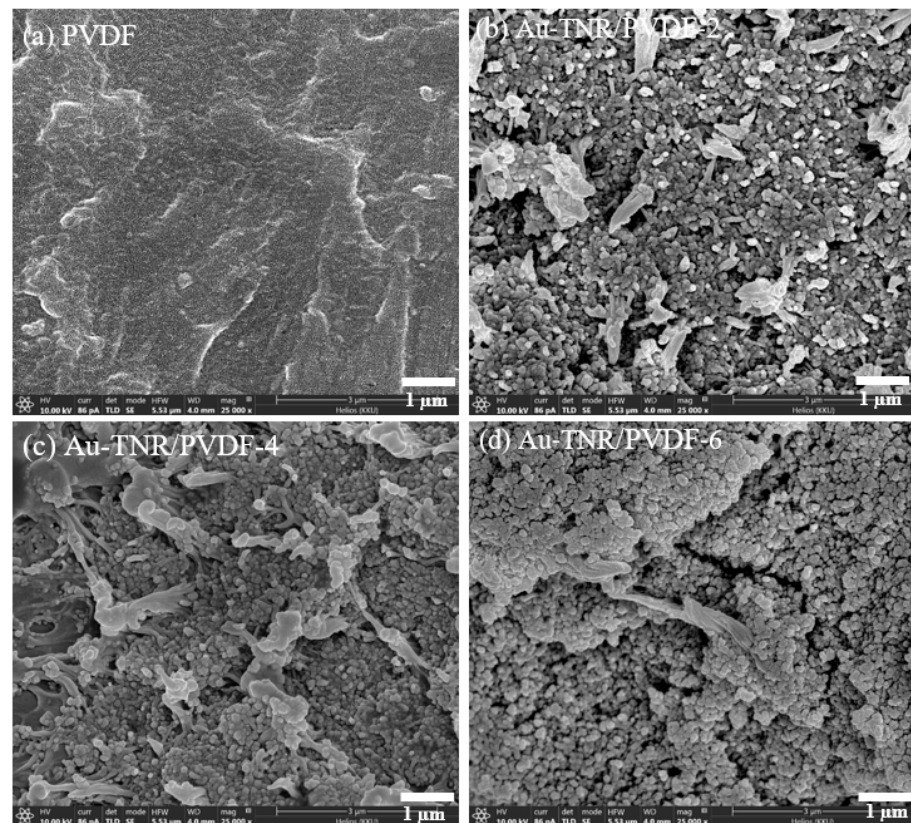


Figure 5. SEM cross-section images of (a) PVDF, (b) Au-TNR/PVDF-2, (c) Au-TNR/PVDF-4, and (d) Au-TNR/PVDF-6.

SEM element maps and EDS were employed to further confirm the existence of Au in the three-phase nanocomposites. As shown in Figure 6, the microstructure of Au-TNR/PVDF-4 exhibited Au clusters dispersed on the TNR surfaces that are surrounded by the PVDF matrix. EDS was used to determine that Au, Ti, O, C, and F are present in the nanocomposite at levels of 1.3, 57, 24.5, 14.3, and 2.9 wt%, respectively.

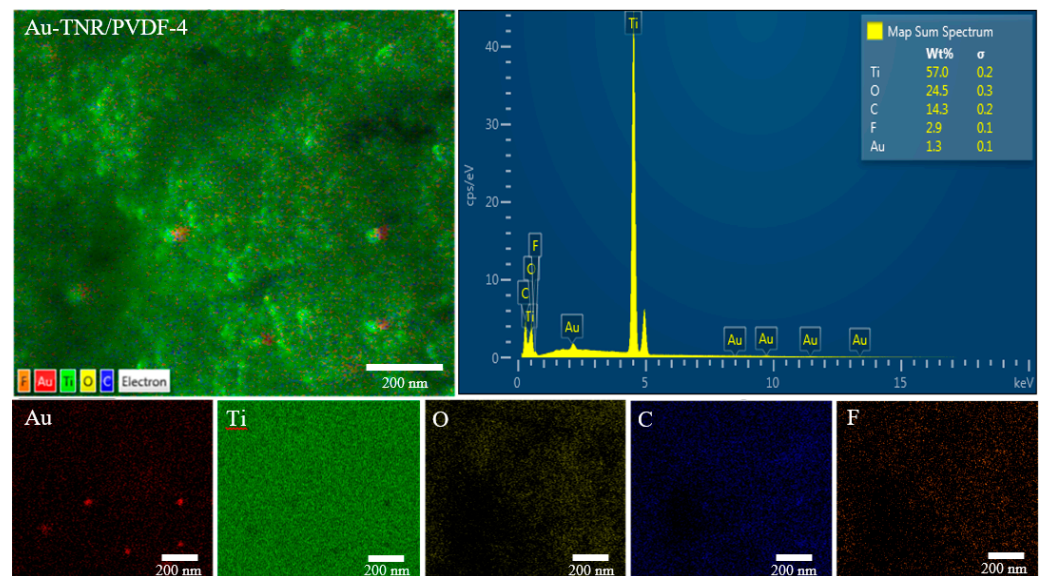


Figure 6. Element mapping and EDS-FESEM characterization of Au-TNR/PVDF-4.

The frequency dependences of ϵ' , $\tan\delta$, and σ_{ac} of nanocomposites with different volume fractions of Au-TNRs ($f_{Au-TNRs}$) at room temperature are shown in Figure 7. As shown in Figure 7a, the ϵ' increased with increasing $f_{Au-TNRs}$. A significant enhancement in ϵ' was achieved by incorporating small amounts of Au and TNR nanoparticles in the nanocomposite. The enhanced ϵ' value of the Au-TNR/PVDF-6 composite was ~ 226 at 1 kHz, which is ~ 20 times larger than that of a pure PVDF polymer ($\epsilon' \approx 10.78$). The increase in ϵ' for the three-phase Au-TNR/PVDF nanocomposites can be ascribed to the formation of Au-TNR hybrid nanoparticles. A large amount of blocked charges at the interface between TNR-PVDF and Au-PVDF can enhance interfacial polarization, which is known as Maxwell–Wagner–Sillars (MWS) polarization [6,46]. Therefore, in an electric field, the enhanced interfacial polarization enhances the ϵ' of the Au-TNR/PVDF nanocomposites. Another factor is the semiconductor nature of the TNR nanoparticles, which can produce interfacial polarization over a wide range of frequencies. Moreover, the ϵ' behavior of each sample exhibits a similar trend in the 10^2 – 10^6 Hz range. Meanwhile, the $\tan\delta$ values of the Au-TNR/PVDF nanocomposites decreased as the frequency was increased to approximately 10^4 kHz and gradually increased at higher frequencies, as shown in Figure 7b. This increase in $\tan\delta$ is generally consistent with the dielectric relaxation of the pure PVDF polymer [6]. Considering a low-frequency range, $\tan\delta$ of the Au-TNR/PVDF nanocomposites increased with increasing $f_{Au-TNRs}$. The increased $\tan\delta$ value as a result of increased filler loading is attributed to the conduction of free charge carriers [6,47], which corresponds to the increase in $f_{Au-TNRs}$. Furthermore, for the composites with high filler loading, it is observed that $\tan\delta$ continuously increases with decreasing frequency from 10^3 to 10^2 Hz. This observation was resulted from the conduction of free charge carriers, which is more prominent in a low-frequency range. The increase in $\tan\delta$ in the high-frequency range is attributed to the α_a relaxation from the glass transition in the PVDF polymer [6,48]. The $\tan\delta$ of the nanocomposite increases slowly with increasing Au-TNR content. Interestingly, $\tan\delta$ is exceptionally low for all nanocomposites at 1 kHz. The maximum value of $\tan\delta$ is less than 0.08 at a frequency of 1 kHz. The $\tan\delta$ value of Au-TNR/PVDF-6 is 0.05, which is much lower than values obtained in other work ($\tan\delta > 0.1$) that used $Ag@TiO_2$ as fillers [34,35,37,49]. As shown in Figure 7c, the σ_{ac} value of the Au-TNR/PVDF nanocomposite increased slightly with increasing Au-TNR content. At $f_{Au-TNRs} = 0.624$, the σ_{ac} value of the nanocomposite was only $6.58 \times 10^{-9} \text{ S}\cdot\text{cm}^{-1}$ at 1 kHz, which is lower than that of the other three-phase composite systems ($>10^{-7} \text{ S}\cdot\text{cm}^{-1}$) [34,35]. These results confirm that no conducting network is formed, indicating that the Au-TNR-PVDF nanocomposites exhibit good insulation properties.

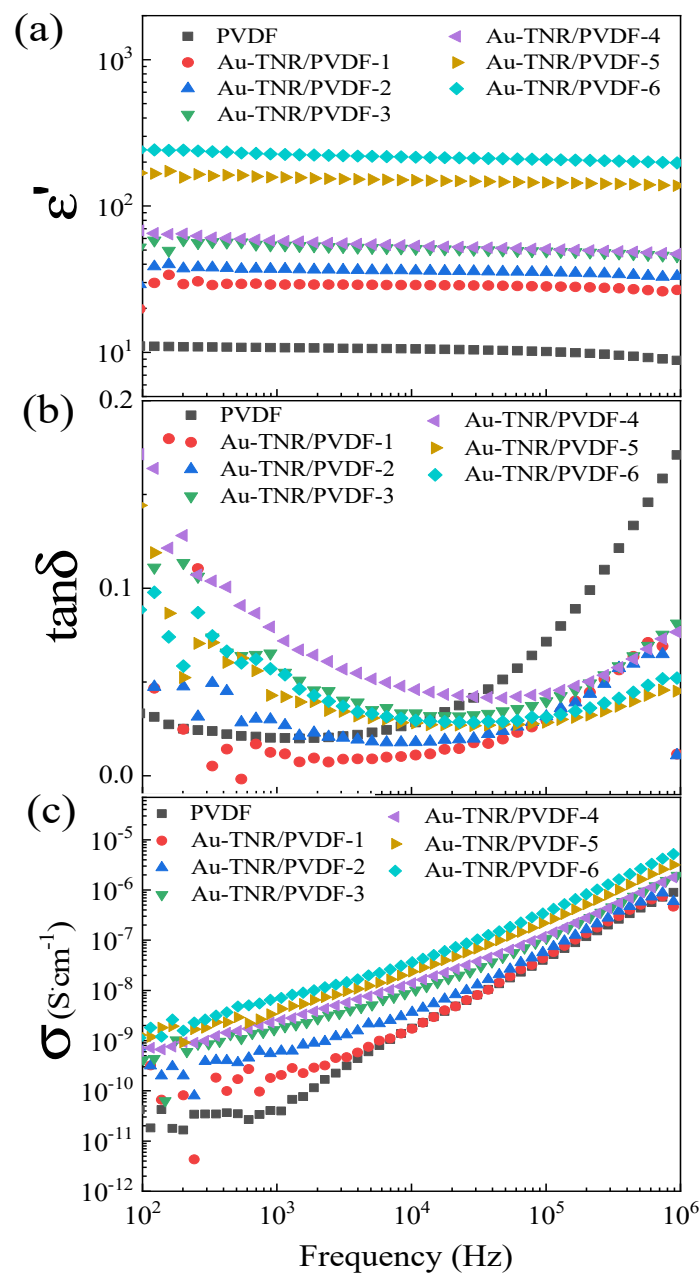


Figure 7. Frequency dependence of (a) ϵ' , (b) $\tan\delta$, and (c) σ for nanocomposites with varying amounts of Au-TNRs.

Figure 8 shows the ϵ' and $\tan\delta$ of Au-TNR/PVDF at 1 kHz as functions of temperature. As shown in Figure 8a, steady values of ϵ' were observed for almost all nanocomposites with increasing temperature. Only Au-TNR/PVDF-5 and Au-TNR/PVDF-6 exhibited ϵ' values that were slightly temperature dependent. Figure 8b shows the $\tan\delta$ relaxation peaks in the pure PVDF polymer. The first relaxation was observed between -40 and 0 °C, which can be attributed to the β -relaxation of PVDF. The second relaxation was observed at a temperature above 40 °C, which can be attributed to the α -relaxation [50].

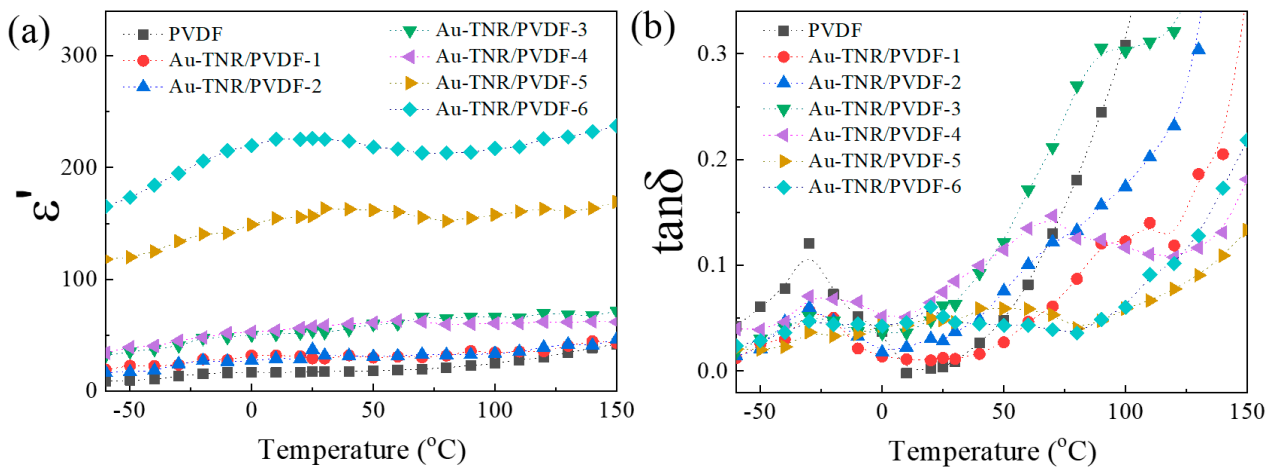


Figure 8. Temperature dependence of (a) ϵ' and (b) $\tan\delta$ for nanocomposites with varying amounts of Au-TNRs.

Figure 9a shows the ϵ' values of TNR/PVDF and Au-TNR/PVDF-5 as a function of frequency. The ϵ' value of the three-phase nanocomposite (Au-TNR/PVDF-5) was found to be much higher than that of the two-phase nanocomposite (TNR/PVDF) (with nearly the same total volume fraction of filler) in the 10^2 – 10^6 Hz frequency range, which indicates that the addition of a small amount of Au nanoparticles can result in a significant enhancement in the ϵ' of a polymer composite. Interestingly, the $\tan\delta$ value of the Au-TNR/PVDF-5 nanocomposite at 1 kHz was 0.048. These excellent dielectric properties of Au-TNR/PVDF are not only due to the introduction of the Au-TNR hybrid nanoparticles, but also due to the increasing polar β -phase in the PVDF matrix, which was confirmed by FTIR spectroscopy (Figure 4). The large interfacial area of the semiconducting TNRs is one of the most important factors that significantly increases the dielectric response in the nanocomposite. As shown in Figure 9b, although $\tan\delta$ of the Au-TNR/PVDF-5 nanocomposite was increased over the measured frequency range compared to that of the two-phase TNR/PVDF nanocomposite, the obtained $\tan\delta$ value was lower than 0.08 in the frequency range of 10^2 – 10^6 Hz.

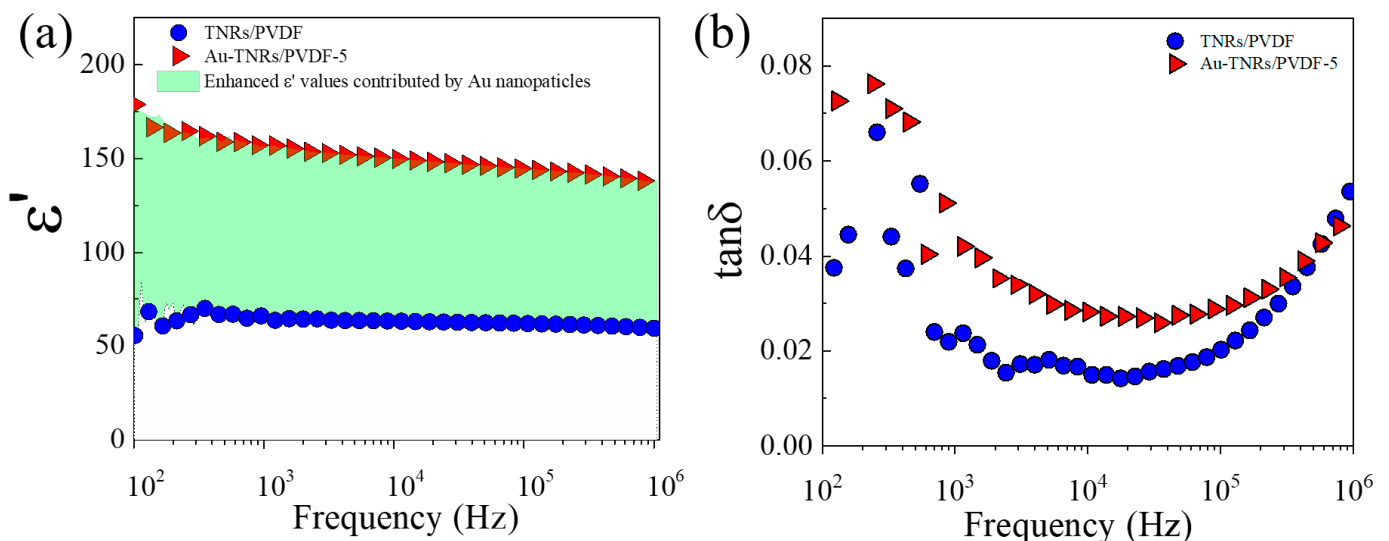


Figure 9. Frequency dependence of (a) ϵ' and (b) $\tan\delta$ for TNR/PVDF and Au-TNR/PVDF-5 at 20 °C; the different ϵ' values (green area) resulted from the Au nanoparticles.

The ϵ' values of the Au-TNR/PVDF nanocomposites could not be fitted to two-phase composite models consisting of a ceramic and a polymer (e.g., effective medium theory (EMT), Maxwell–Garnett, Yamada, logarithmic [5,51]) with high Au-TNR contents, as

demonstrated in the inset of Figure 10. This is due to interfacial polarization at the interface between fillers and PVDF polymer matrix. Moreover, the ϵ' values of the Au-TNR/PVDF nanocomposites could not be fitted to the percolation model, which is employed for metal/polymer dual phases. As shown in Figure 10, the dielectric behavior of the Au-TNR/PVDF nanocomposites is in good agreement with the EMPT model [35,52], which combines the EMT model with percolation theory, as shown in Equation (4):

$$\epsilon_{\text{eff}} = \epsilon_{\text{PVDF}} \left[1 + \frac{f_{\text{TNRs}}(\epsilon_{\text{TNRs}} - \epsilon_{\text{PVDF}})}{\epsilon_{\text{PVDF}} + n(1 - f_{\text{TNRs}})(\epsilon_{\text{TNRs}} - \epsilon_{\text{PVDF}})} \right] \left| \frac{f_c - f}{f} \right|^{-q} \quad (4)$$

where ϵ_{eff} is the effective ϵ' of the Au-TNR/PVDF composite, f_{TNRs} is the volume fraction of the TNRs, f_c is the percolation threshold, ϵ_{PVDF} is the ϵ' of PVDF ($\epsilon_{\text{PVDF}} = 10.78$), ϵ_{TNRs} is the ϵ' of TNRs ($\epsilon_{\text{TNRs}} = 150$), n is the morphology fitting factor, and q is the critical exponent. Due to the semiconducting nature of TNRs and conducting nature of Au nanoparticles, f is assigned as the volume fraction of Au-TNR hybrid particles, which can influence the percolation behavior of the composites. For the curve fitted using the EMPT model, the optimum fitting parameters were determined to be: $n = 0.11$, $q = 1.0$, and $f_c = 0.8$. It is worth noting that n and q are very close to those reported for the Ag-BaTiO₃/PVDF ($n = 0.11$) [52] and the Ni-BaTiO₃/PVDF ($q = 1.0$) [23], respectively. The percolation threshold is expected to occur at a high filler loading ($f_c = 0.8$), which is much higher than the maximum filler loading used in this current study, and is due to the small amount of conductive Au nanoparticles used and the hybrid structure of the Au-TNR particles. Therefore, the percolation network (or conduction pathway) would not be formed in the Au-TNR/PVDF composite because the hybrid structures of the Au-TNRs prevent the formation of conducting pathways because the randomly grown Au nanoparticles do not continuously coat the TNR surface. The large increase in the ϵ' value is primarily attributed to interfacial polarization between the Au–PVDF, Au–TNR, and TNR–PVDF interfaces.

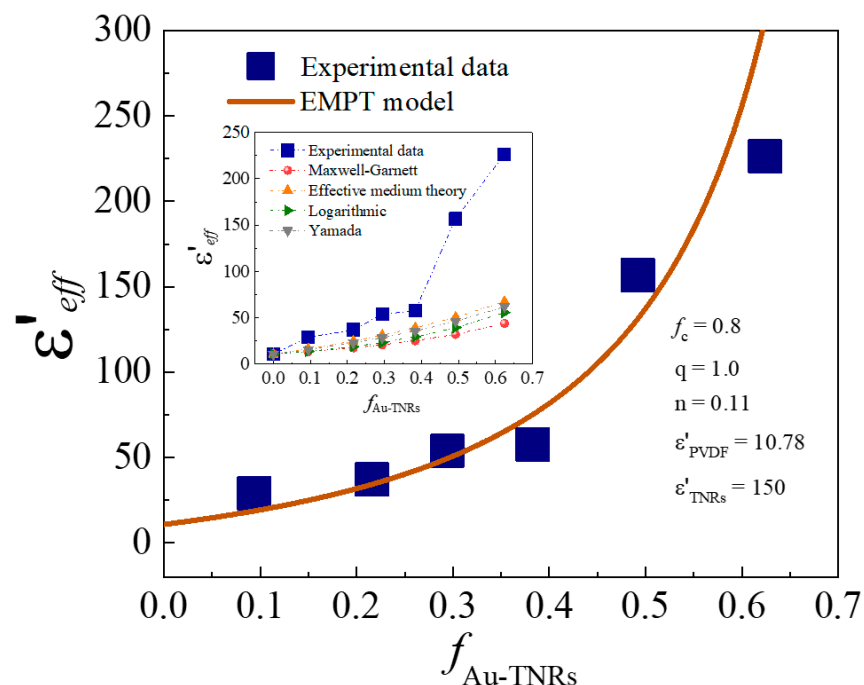


Figure 10. Experimental data of ϵ' for the Au-TNR/PVDF nanocomposites at 1 kHz and 20 °C fitted by the effective medium theory (EMPT) model; inset is the experimental data of ϵ' for the Au-TNR/PVDF nanocomposites fitted by two-phase various theoretical models.

4. Conclusions

This study presented a novel method for successfully achieving high ϵ' and low $\tan\delta$ in three-phase PVDF polymer-matrix nanocomposites. The dielectric properties of a PVDF polymer improved significantly by incorporating conductive Au nanoparticles and semi-conductive TNRs with enlarged interfacial areas. The Au nanoparticles were discretely attached to the TNR surfaces to enhance interfacial polarization and simultaneously prevent the formation of conducting pathways in the insulative PVDF matrix. As a result, a high ϵ' (~157) and low $\tan\delta$ (~0.05) were obtained in the three-phase nanocomposite filled with 1.8 vol% Au and 47.4 vol% TNRs. The dielectric response in the two-phase TNR/PVDF composite increased by more than a factor of two after introducing small amounts of Au nanoparticles. This dielectric behavior is described using the EMPT model. The results indicate that Au nanoparticles significantly contribute to enhancing interfacial polarization and creating a more polar β -PVDF phase, which increases ϵ' . In contrast, due to the small amount of Au nanoparticles used and their discrete growth on the TNRs, the value of $\tan\delta$ remained low. To further investigate the possible use of the Au-TNR/PVDF nanocomposites in capacitor applications, fabrication conditions that produce nanocomposite thin films need be studied.

Author Contributions: Conceptualization, P.K.-o., and P.T.; Formal analysis, P.K.-o. and P.T.; Funding acquisition, P.C.; Investigation, P.K.-o., N.C., J.M., V.H., and N.P.; Methodology, P.K.-o.; Visualization, P.K.-o.; Writing—original draft, P.K.-o. and P.T.; Writing—review & editing, P.T. All authors have read and agreed to the published version of the manuscript.

Funding: This research was funded by the Research and Graduate Studies and the Basic Research Fund of Khon Kaen University, grant number 1500147. This work was funded by the Synchrotron Light Research Institute, Khon Kaen University, and the Thailand Research Fund (TRF), grant number BRG6180003 and the Post-doctoral Program from Research Affairs and Graduate School, Khon Kaen University, grant number 60170. It was partially supported by the Research Network NANOTEC (RNN) program of the National Nanotechnology Center (NANOTEC), NSTDA, Ministry of Higher Education, Science, Research, and Innovation (MHESI), grant number P1851882.

Institutional Review Board Statement: Not applicable.

Informed Consent Statement: Not applicable.

Data Availability Statement: The data presented in this study are available in article.

Acknowledgments: This research was supported by Research and Graduate Studies and the Basic Research Fund of Khon Kaen University (Grant No. 1500147). This work was partially supported by the Synchrotron Light Research Institute, Khon Kaen University, and the Thailand Research Fund (TRF) (Grant No. BRG6180003). This work also received a scholarship under the Post-doctoral Program from Research Affairs and Graduate School, Khon Kaen University (60170). It was partially supported by the Research Network NANOTEC (RNN) program of the National Nanotechnology Center (NANOTEC), NSTDA, Ministry of Higher Education, Science, Research, and Innovation (MHESI) (Grant No. P1851882), and Khon Kaen University, Thailand. P.K. would like to thank the Science Achievement Scholarship of Thailand (SAST).

Conflicts of Interest: The authors declare no conflict of interest.

References

1. Zhang, S.; Zhang, N.; Huang, C.; Ren, K.; Zhang, Q.M. Microstructure and electromechanical properties of carbon nanotube/poly(vinylidene fluoride—trifluoroethylene—chlorofluoroethylene) composites. *Adv. Mater.* **2005**, *17*, 1897–1901. [[CrossRef](#)]
2. Beier, C.W.; Sanders, J.M.; Brutche, R.L. Improved breakdown strength and energy density in thin-film polyimide nanocomposites with small barium strontium titanate nanocrystal fillers. *J. Phys. Chem. C* **2013**, *117*, 6958–6965. [[CrossRef](#)]
3. Thakur, V.K.; Gupta, R.K. Recent progress on ferroelectric polymer-based nanocomposites for high energy density capacitors: Synthesis, dielectric properties, and future aspects. *Chem. Rev.* **2016**, *116*, 4260–4317.
4. Martins, P.; Lopes, A.C.; Lanceros-Mendez, S. Electroactive phases of poly(vinylidene fluoride): Determination, processing and applications. *Prog. Polym. Sci.* **2014**, *39*, 683–706. [[CrossRef](#)]
5. Thomas, P.; Varughese, K.T.; Dwarakanath, K.; Varma, K.B.R. Dielectric properties of poly(vinylidene fluoride)/cacu3ti4o12 composites. *Compos. Sci. Technol.* **2010**, *70*, 539–545. [[CrossRef](#)]

6. Yu, K.; Niu, Y.; Zhou, Y.; Bai, Y.; Wang, H.; Randall, C. Nanocomposites of surface-modified batio₃nanoparticles filled ferroelectric polymer with enhanced energy density. *J. Am. Ceram. Soc.* **2013**, *96*, 2519–2524. [[CrossRef](#)]
7. Huang, X.; Jiang, P.; Xie, L. Ferroelectric polymer/silver nanocomposites with high dielectric constant and high thermal conductivity. *Appl. Phys. Lett.* **2009**, *95*, 242901. [[CrossRef](#)]
8. Wang, L.; Dang, Z.-M. Carbon nanotube composites with high dielectric constant at low percolation threshold. *Appl. Phys. Lett.* **2005**, *87*, 042903. [[CrossRef](#)]
9. Moharana, S.; Mahaling, R.N. Preparation and properties of benzoxazine (ba) based bifeo₃-poly(vinylidene fluoride) (pvdf) composites: Enhanced dielectric constant and suppressed loss. *Polym. Plast. Technol. Mater.* **2021**, *60*, 1122–1134.
10. Kishor Kumar, M.J.; Kalathi, J.T. Investigation on the dielectric performance of pvdf-hfp/lzo composites. *J. Alloy. Compd.* **2020**, *843*, 155889.
11. Zhang, Y.; Wang, W.; Zhang, J.; Ni, Y. Dielectric relaxation processes in pvdf composite. *Polym. Test.* **2020**, *91*, 106801. [[CrossRef](#)]
12. Thomas, P.; Satapathy, S.; Dwarakanath, K.; Varma, K.B.R. Dielectric properties of poly(vinylidene fluoride)/cacu₃ti₄o₁₂ nanocrystal composite thick films. *Express Polym. Lett.* **2010**, *4*, 632–643. [[CrossRef](#)]
13. Amaral, F.; Rubinger, C.P.L.; Henry, F.; Costa, L.C.; Valente, M.A.; Barros-Timmons, A. Dielectric properties of polystyrene-ccto composite. *J. Non Cryst. Solids* **2008**, *354*, 5321–5322. [[CrossRef](#)]
14. Zhang, L.; Wu, P.; Li, Y.; Cheng, Z.Y.; Brewer, J.C. Preparation process and dielectric properties of ba_{0.5}sr_{0.5}ti₃-p(vdf-ctfe) nanocomposites. *Compos. Part B Eng.* **2014**, *56*, 284–289. [[CrossRef](#)]
15. Li, K.; Wang, H.; Xiang, F.; Liu, W.; Yang, H. Surface functionalized ba_{0.6}sr_{0.4}ti₃ /poly(vinylidene fluoride) nanocomposites with significantly enhanced dielectric properties. *Appl. Phys. Lett.* **2009**, *95*, 202904. [[CrossRef](#)]
16. Su, Y.-L.; Sun, C.; Zhang, W.-Q.; Huang, H. Fabrication and dielectric properties of na_{0.5}bi_{0.5}cu₃ti₄o₁₂/poly(vinylidene fluoride) composites. *J. Mater. Sci.* **2013**, *48*, 8147–8152. [[CrossRef](#)]
17. Dang, Z.M.; Lin, Y.H.; Nan, C.W. Novel ferroelectric polymer composites with high dielectric constants. *Adv. Mater.* **2003**, *15*, 1625–1629. [[CrossRef](#)]
18. Zhang, L.; Bass, P.; Cheng, Z.Y. Revisiting the percolation phenomena in dielectric composites with conducting fillers. *Appl. Phys. Lett.* **2014**, *105*, 042905. [[CrossRef](#)]
19. Begum, S.; Ullah, H.; Kausar, A.; Siddiq, M.; Aleem, M.A. Fabrication of epoxy functionalized mwcnts reinforced pvdf nanocomposites with high dielectric permittivity, low dielectric loss and high electrical conductivity. *Compos. Sci. Technol.* **2018**, *167*, 497–506. [[CrossRef](#)]
20. Audoit, J.; Laffont, L.; Lonjon, A.; Dantras, E.; Lacabanne, C. Percolative silver nanoplates/pvdf nanocomposites: Bulk and surface electrical conduction. *Polymer* **2015**, *78*, 104–110. [[CrossRef](#)]
21. Wang, Z.; Wang, T.; Fang, M.; Wang, C.; Xiao, Y.; Pu, Y. Enhancement of dielectric and electrical properties in bfn/ni/pvdf three-phase composites. *Compos. Sci. Technol.* **2017**, *146*, 139–146. [[CrossRef](#)]
22. Yang, W.; Yu, S.; Sun, R.; Ke, S.; Huang, H.; Du, R. Electrical modulus analysis on the ni/ccto/pvdf system near the percolation threshold. *J. Phys. D Appl. Phys.* **2011**, *44*, 475305. [[CrossRef](#)]
23. Dang, Z.M.; Shen, Y.; Nan, C.W. Dielectric behavior of three-phase percolative ni-batio₃/polyvinylidene fluoride composites. *Appl. Phys. Lett.* **2002**, *81*, 4814–4816. [[CrossRef](#)]
24. Su, Y.; Gu, Y.; Feng, S. Composites of nbcto/mwcnts/pvdf with high dielectric permittivity and low dielectric loss. *J. Mater. Sci. Mater. Electron.* **2017**, *29*, 2416–2420. [[CrossRef](#)]
25. Su, Y.; Gu, Y.; Li, H.; Geng, F. Ag-nbcto-pvdf composites with enhanced dielectric properties. *Mater. Lett.* **2016**, *185*, 208–210. [[CrossRef](#)]
26. Luo, S.; Yu, S.; Sun, R.; Wong, C.P. Nano ag-deposited batio₃ hybrid particles as fillers for polymeric dielectric composites: Toward high dielectric constant and suppressed loss. *ACS Appl. Mater. Interfaces* **2014**, *6*, 176–182. [[CrossRef](#)]
27. Arbatti, M.; Shan, X.; Cheng, Z.Y. Ceramic-polymer composites with high dielectric constant. *Adv. Mater.* **2007**, *19*, 1369–1372. [[CrossRef](#)]
28. Hu, W.; Liu, Y.; Withers, R.L.; Frankcombe, T.J.; Noren, L.; Snashall, A.; Kitchin, M.; Smith, P.; Gong, B.; Chen, H.; et al. Electron-pinned defect-dipoles for high-performance colossal permittivity materials. *Nat. Mater.* **2013**, *12*, 821–826. [[CrossRef](#)] [[PubMed](#)]
29. Homes, C.C.; Vogt, T. Colossal permittivity materials: Doping for superior dielectrics. *Nat. Mater.* **2013**, *12*, 782–783. [[CrossRef](#)]
30. Tuichai, W.; Danwittayakul, S.; Chanlek, N.; Thongbai, P. Nonlinear current-voltage and giant dielectric properties of al³⁺ and ta⁵⁺ co-doped tio₂ ceramics. *Mater. Res. Bull.* **2019**, *116*, 137–142. [[CrossRef](#)]
31. Tse, M.-Y.; Wei, X.; Wong, C.-M.; Huang, L.-B.; Lam, K.-H.; Dai, J.; Hao, J. Enhanced dielectric properties of colossal permittivity co-doped tio₂/polymer composite films. *RSC Adv.* **2018**, *8*, 32972–32978. [[CrossRef](#)]
32. Kim, K. Characterization of poly(vinylidene fluoride-co-hexafluoropropylene)-based polymer electrolyte filled with rutile tio₂ nanoparticles. *Solid State Ion.* **2003**, *161*, 121–131. [[CrossRef](#)]
33. An, N.; Liu, H.; Ding, Y.; Zhang, M.; Tang, Y. Preparation and electroactive properties of a pvdf/nano-tio₂ composite film. *Appl. Surf. Sci.* **2011**, *257*, 3831–3835. [[CrossRef](#)]
34. Chen, X.; Liang, F.; Lu, W.; Zhao, Y.; Fan, G.; Wang, X. Improved dielectric properties of ag@tio₂/pvdf nanocomposites induced by interfacial polarization and modifiers with different carbon chain lengths. *Appl. Phys. Lett.* **2018**, *112*, 162902. [[CrossRef](#)]

35. Liang, F.; Zhang, L.; Lu, W.-Z.; Wan, Q.-X.; Fan, G.-F. Dielectric performance of polymer-based composites containing core-shell ag@tio₂ nanoparticle fillers. *Appl. Phys. Lett.* **2016**, *108*, 072902. [[CrossRef](#)]
36. Yang, D.; Huang, S.; Ruan, M.; Wu, Y.; Li, S.; Wang, H.; Zhang, J.; Ma, H.; Guo, W.; Zhang, L. Controllable dielectric performance of polymer composites via the coulomb-blockade effect with core-shell structured nano-particles. *J. Mater. Chem. C* **2017**, *5*, 7759–7767. [[CrossRef](#)]
37. Xu, N.; Xiao, X.; Yang, H.; Yu, E.; Zhang, Q. Enhanced dielectric constant and suppressed dielectric loss of ternary composites based on ag-p(vdf-hfp) matrix and tio₂ nanowires. *Ceram. Int.* **2016**, *42*, 12475–12481. [[CrossRef](#)]
38. Daniel, M.C.; Astruc, D. Gold nanoparticles: Assembly, supramolecular chemistry, quantum-size-related properties, and applications toward biology, catalysis, and nanotechnology. *Chem. Rev.* **2004**, *104*, 293–346. [[CrossRef](#)]
39. Phromviyo, N.; Thongbai, P.; Maensiri, S. High dielectric permittivity and suppressed loss tangent in pvdf polymer nanocomposites using gold nanoparticle-deposited batio₃ hybrid particles as fillers. *Appl. Surf. Sci.* **2018**, *446*, 236–242. [[CrossRef](#)]
40. Kum-onsa, P.; Chanlek, N.; Putasaeng, B.; Thongbai, P. Improvement in dielectric properties of poly(vinylidene fluoride) by incorporation of au-bifeo₃ hybrid nanoparticles. *Ceram. Int.* **2020**, *46*, 17272–17279. [[CrossRef](#)]
41. Pramanik, G.; Humpolickova, J.; Valenta, J.; Kundu, P.; Bals, S.; Bour, P.; Dracinsky, M.; Cigler, P. Gold nanoclusters with bright near-infrared photoluminescence. *Nanoscale* **2018**, *10*, 3792–3798. [[CrossRef](#)] [[PubMed](#)]
42. Zhou, C.; Sun, C.; Yu, M.; Qin, Y.; Wang, J.; Kim, M.; Zheng, J. Luminescent gold nanoparticles with mixed valence states generated from dissociation of polymeric au (i) thiolates. *J. Phys. Chem. C Nanomater. Interfaces* **2010**, *114*, 7727–7732. [[CrossRef](#)]
43. Liu, G.; Fan, H.; Xu, J.; Liu, Z.; Zhao, Y. Colossal permittivity and impedance analysis of niobium and aluminum co-doped tio₂ ceramics. *RSC Adv.* **2016**, *6*, 48708–48714. [[CrossRef](#)]
44. Ribeiro, C.; Costa, C.M.; Correia, D.M.; Nunes-Pereira, J.; Oliveira, J.; Martins, P.; Gonçalves, R.; Cardoso, V.F.; Lanceros-Méndez, S. Electroactive poly(vinylidene fluoride)-based structures for advanced applications. *Nat. Protoc.* **2018**, *13*, 681–704. [[CrossRef](#)]
45. Kumar, S.; Supriya, S.; Kar, M. Enhancement of dielectric constant in polymer-ceramic nanocomposite for flexible electronics and energy storage applications. *Compos. Sci. Technol.* **2018**, *157*, 48–56. [[CrossRef](#)]
46. Ren, L.; Meng, X.; Zha, J.-W.; Dang, Z.-M. Coulomb block effect inducing distinctive dielectric properties in electroless plated barium titanate@silver/poly(vinylidene fluoride) nanocomposites. *RSC Adv.* **2015**, *5*, 65167–65174. [[CrossRef](#)]
47. Chen, G.; Wang, X.; Lin, J.; Yang, W.; Li, H.; Wen, Y. Interfacial polarity modulation of kta_{0.5}nb_{0.5}o₃ nanoparticles and its effect on dielectric loss and breakdown strength of poly(vinylidene fluoride) nanocomposites with high permittivity. *J. Phys. Chem. C* **2016**, *120*, 28423–28431. [[CrossRef](#)]
48. Song, Y.; Shen, Y.; Hu, P.; Lin, Y.; Li, M.; Nan, C.W. Significant enhancement in energy density of polymer composites induced by dopamine-modified ba_{0.6}sr_{0.4}tio₃ nanofibers. *Appl. Phys. Lett.* **2012**, *101*, 152904. [[CrossRef](#)]
49. Dang, Z.-M.; You, S.-S.; Zha, J.-W.; Song, H.-T.; Li, S.-T. Effect of shell-layer thickness on dielectric properties in ag@tio₂core@shell nanoparticles filled ferroelectric poly(vinylidene fluoride) composites. *Phys. Status Solidi A* **2010**, *207*, 739–742. [[CrossRef](#)]
50. Lopes, A.C.; Costa, C.M.; Serra, R.S.i.; Neves, I.C.; Ribelles, J.L.G.; Lanceros-Méndez, S. Dielectric relaxation, ac conductivity and electric modulus in poly(vinylidene fluoride)/nay zeolite composites. *Solid State Ion.* **2013**, *235*, 42–50. [[CrossRef](#)]
51. Chen, G.; Yang, W.; Lin, J.; Wang, X.; Li, D.; Wang, Y.; Liang, M.; Ding, W.; Li, H.; Lei, Q. Geometrical shape adjustment of kta_{0.5}nb_{0.5}o₃ nanofillers for tailored dielectric properties of kta_{0.5}nb_{0.5}o₃/pvdf composite. *J. Mater. Chem. C* **2017**, *5*, 8135–8143. [[CrossRef](#)]
52. Fang, F.; Yang, W.; Yu, S.; Luo, S.; Sun, R. Mechanism of high dielectric performance of polymer composites induced by batio₃-supporting ag hybrid fillers. *Appl. Phys. Lett.* **2014**, *104*, 132909. [[CrossRef](#)]